


## Rydberg excitation spectrum of $^{40}\text{K}$ ultracold Fermi gases

Donghao Li,<sup>1,2</sup> Guoqi Bian,<sup>1,2</sup> Jie Miao,<sup>1,2</sup> Pengjun Wang,<sup>1,2</sup> Zengming Meng,<sup>1,2</sup>  
Liangchao Chen,<sup>1,2</sup> Lianghui Huang <sup>1,2,\*</sup> and Jing Zhang<sup>1,†</sup>

<sup>1</sup>State Key Laboratory of Quantum Optics and Quantum Optics Devices, Institute of Opto-electronics,  
Shanxi University, Taiyuan, Shanxi 030006, People's Republic of China

<sup>2</sup>Collaborative Innovation Center of Extreme Optics, Shanxi University, Taiyuan, Shanxi 030006, People's Republic of China



(Received 28 January 2021; revised 29 May 2021; accepted 1 June 2021; published 14 June 2021)

We report the measurement of the Rydberg excitation spectrum by two-photon process in ultracold  $^{40}\text{K}$  Fermi gases. Two different methods are employed to measure the Rydberg excitation spectrum, depending on the power of the probe laser. One scheme is to reduce atomic losses by means of electromagnetically induced transparency. The other is to enhance the atomic losses by spontaneous avalanche ionization due to the strong Rydberg-Rydberg interactions. We verify the consistency of both of the methods. The highest Rydberg states detectable in our experiment are limited to  $n \leq 62$  due to the competition between the long Rydberg blockade effective range and the limited atomic cloud size.

DOI: [10.1103/PhysRevA.103.063305](https://doi.org/10.1103/PhysRevA.103.063305)

Due to their long lifetimes, large cross sections, very large polarizabilities, etc. [1], the Rydberg atoms are extremely sensitive to external electric and magnetic fields and exhibit strong atom-atom interactions and large optical nonlinearities. Under ultracold conditions, the thermal motion can be neglected and the long-range dipole-dipole interactions play a major role. This interaction manifest in a variety of phenomena, including the excitation-blockade effect [2,3], exotic molecules (trilobite Rydberg molecules [4–6], butterfly Rydberg molecules [7,8], macrodimers [9–13]), and in few-body to many-body physics between one Rydberg atom and multiple ground-state atoms [14]. The Rydberg atom is an ideal system for the implementation of highly controllable quantum simulators [15–19], because the interactions can be controlled by static electric or magnetic, laser or microwave fields.

Since a Rydberg atom interacting with an ultracold background atomic gas leads to the formation of a molecular shell structure in the quantum regime, the bosonic or fermionic quantum statistics will play an important role [20,21]. The first evidence of the Fermi suppression has been observed in a nondegenerate Fermi gas of  $^{87}\text{Sr}$  [22]. Rydberg-dressed atomic gases display the rich many-body phenomena [23,24]. Many phenomena relating to the Rydberg states have been studied experimentally in an atomic Bose-Einstein condensate [11,25–32] and theoretically predicted in degenerate Fermi gases [33–38]; however, the degenerate Fermi gases are still waiting to be studied and explored experimentally. The experimental realization of Rydberg-dressed interactions between fermionic atoms would be an exciting step toward resolving puzzles related to strongly correlated electronic solids, such as topological superfluids [34] and topological density wave

[35]. Among the alkali-metal atoms, potassium is the element with three naturally abundant isotopes: Boson  $^{39}\text{K}$ ,  $^{41}\text{K}$ , and fermion  $^{40}\text{K}$ .  $^{40}\text{K}$  atoms are an attractive candidate for Rydberg dressing of a fermionic species because they are readily obtained degenerate Fermi gases. Rydberg excitation spectroscopy of boson  $^{39}\text{K}$  has been carried out experimentally in [39–41]. The natural abundance of fermionic  $^{40}\text{K}$  is very low and the measurement of Rydberg excitation spectra for fermionic  $^{40}\text{K}$  atoms is not easy to perform. In this paper, we measure the Rydberg excitation spectrum by a two-photon process in ultracold  $^{40}\text{K}$  Fermi gas. The Rydberg excitation spectrum is obtained by measuring the atomic losses instead of the transmitted probe beam. Two different methods are employed to measure the spectrum using different powers of the probe laser. One method is to reduce atomic losses by means of electromagnetically induced transparency (EIT) [42] using a low probe power. The second method (the avalanche ionization scheme) is to enhance the atomic losses by spontaneous avalanche ionization [43,44] of the strong Rydberg-Rydberg interactions by using a high power probe beam. We compare the two methods and show that the Rydberg excitation spectrum using both methods agree each other very well. We find that the detectable highest Rydberg state in our experiment is  $n \leq 62$  limited by competition between Rydberg blockade effective range and the atomic cloud size. This work takes the first step to study Rydberg-dressed ultracold  $^{40}\text{K}$  Fermi gases. Moreover, our work provides a platform to generate ultracold strongly coupled plasmas from the degenerate Fermi gases to explore the physics of nonequilibrium dynamics.

The experimental setup and energy level scheme for the two-photon Rydberg excitation are shown in Fig. 1. The three-level ladder-type energy levels include the ground state  $4S_{1/2}$ , intermediate state  $4P_{3/2}$ , and highly excited Rydberg states  $ns$  and  $nd$ . A weak probe beam (red laser) with wavelength 767 nm is locked to the transition between  $|F = 9/2, m_F = 9/2\rangle$  state of  $4S_{1/2}$  and  $|F' = 11/2, m_{F'} = 11/2\rangle$

\*Corresponding author: [huanglh06@sxu.edu.cn](mailto:huanglh06@sxu.edu.cn)

†Corresponding author: [jzhang74@yahoo.com](mailto:jzhang74@yahoo.com);  
[jzhang74@sxu.edu.cn](mailto:jzhang74@sxu.edu.cn)

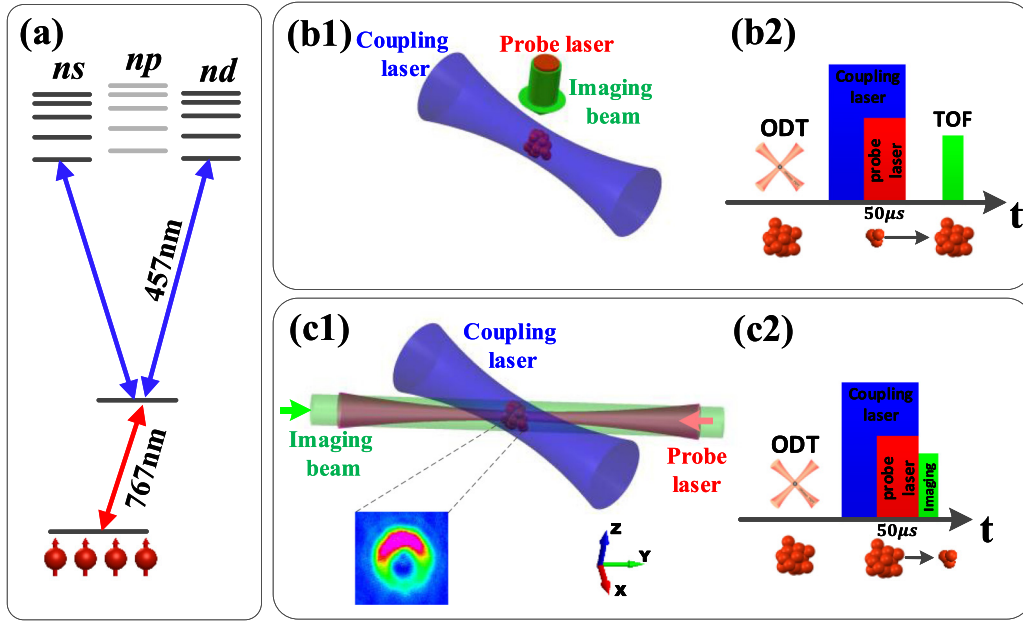


FIG. 1. Experimental setup and procedure. (a) Level scheme of the two-photon excitation of  $^{40}\text{K}$  to Rydberg *ns* and *nd* states. (b), (c) The schematic of the two detection schemes. (b1) The optical setup for the EIT method. The same probe laser is used for the EIT and also, for absorption imaging, propagates along the *z* axis. (b2) The time sequence for the EIT detection method showing the atoms ballistically expand to take the time-of-flight (TOF) absorption image with a CCD. (c1) The avalanche ionization scheme setup. The probe laser propagates along the *y* axis, focused onto the ensemble through a high-NA aspheric lens while a separate nonfocused imaging probe is used for taking the absorption image. The inset shows the *in situ* atomic density in which the hole at the center shows the atomic losses by the strongly focused probe light. (c2) The time sequence for the enhanced atomic losses detection method. The atoms are imaged by *in situ* imaging. Here, the coupling field (blue laser) intersects with the *y* axis at an angle of  $45^\circ$ .

state of  $4P_{3/2}$ . A strong-coupling beam (blue laser) drives the transition between the intermediate  $|F' = 11/2, m_{F'} = 11/2\rangle$  state of  $4P_{3/2}$  and the highly excited Rydberg states *ns* and *nd* at around 457 nm. The coupling laser beam is derived from a system of ECDL (external cavity diode laser)-TA (tapered amplifier)-SHG (cavity-enhanced second harmonic generation) providing 800 mW output at around 457 nm. The frequency of the coupling laser is scanned and measured using a high-resolution wavemeter (HighFinesse, WS7, measurement resolution of 10 MHz). The pulse duration and intensity of the probe and coupling laser beams is controlled through acousto-optic modulators (AOMs).

The experiment starts with the preparation of a degenerate Fermi gas of  $^{40}\text{K}$  atoms in the state  $|F = 9/2, m_F = 9/2\rangle$  in a crossed optical dipole trap. Around  $N = 3 \times 10^6$  ultracold  $^{40}\text{K}$  atoms are prepared at a temperature of  $0.3T_F$  using sympathetic cooling by  $^{87}\text{Rb}$ , where the Fermi temperature is defined by  $T_F = \hbar\bar{\omega}(6N)^{1/3}/k_B$ . Here  $\bar{\omega} = (\omega_x\omega_y\omega_z)^{1/3} \simeq 2\pi \times 80$  Hz is the geometric mean of the optical trap in our experiment,  $N$  is the particle number of  $^{40}\text{K}$  atoms, and  $k_B$  is the Boltzmann's constant. The remaining  $^{87}\text{Rb}$  atoms are removed by shining a resonant laser beam pulse (780 nm) for 0.03 ms without heating and losing  $^{40}\text{K}$  atoms.

Usually, there are two ways to observe the EIT spectrum [46]. The first method is to measure the transmission of a probe beam through an atomic sample via scanning its frequency, while the frequency of the coupling beam is locked [47,48]. This method results in the standard three level EIT line shape, which has a narrow transmission window at the resonance frequency and strong absorption at the two dressed

states on both sides of the transmission window. The other method is to measure the probe beam intensity by scanning the frequency of the coupling beam across the atomic transition and keeping the probe laser locked [49], which can eliminate the Doppler background in thermal vapors [50]. Here, we use the second method to obtain the Rydberg excitation spectrum in ultracold Fermi gases by measuring the atom losses.

First, we measure the spectrum of high-lying Rydberg states using a low power probe laser through the EIT (leading to reduced atomic loss at the Rydberg resonances). The strong-coupling laser will induce the ac Stark shift of the intermediate state  $4P_{3/2}$ . In this scheme, the probe laser propagates along the *z* axis and is collimated with a Gaussian waist of 1 cm, while the coupling laser (in the *xy* plane) is focused on the Fermi atomic cloud with the  $1/e^2$  radius of approximately  $100 \mu\text{m}$  as shown in Fig. 1(b1). The probe and coupling field intensities are around  $I = 1.9 \times 10^{-7} \text{ W/mm}^2$  and  $I = 19 \text{ W/mm}^2$ , respectively. The coupling field is turned on first and after  $50 \mu\text{s}$  the probe field is turned on, which then stays on for  $50 \mu\text{s}$  together with the coupling field after which both are simultaneously turned off. The frequency of the probe field is fixed at the resonance, while the frequency of the coupling laser is scanned as shown in Fig. 1(b2). After exposure to the two fields, we immediately turn off the optical trap and the homogeneous magnetic field, and let the atoms ballistically expand for 12 ms and take the time-of-flight (TOF) absorption image with a CCD. Therefore, the Rydberg excitation spectrum is obtained from the number of remaining atoms in the optical trap as the function of the coupling laser detuning.

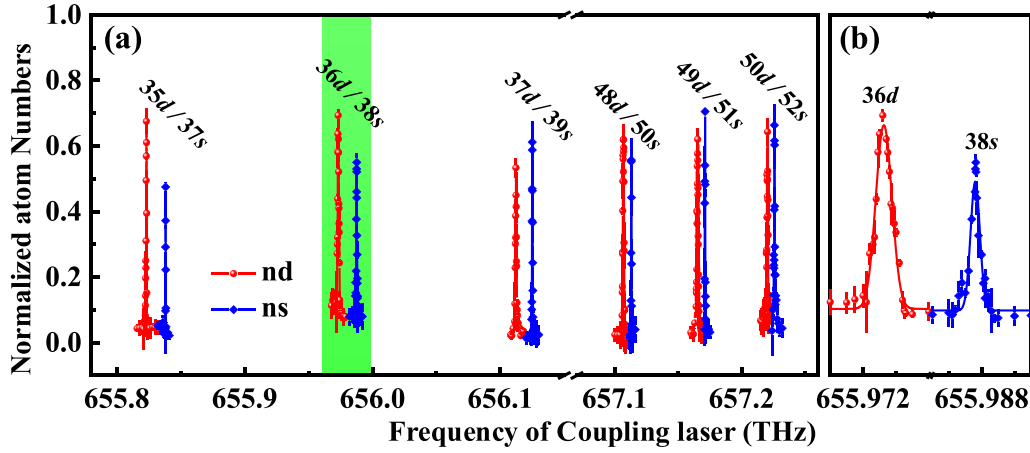


FIG. 2. Rydberg spectrum of ultracold  $^{40}\text{K}$  atoms by the EIT detection scheme. (a) Trap loss Rydberg spectrum as a function of the frequency of the coupling (blue) laser. The spectrum for  $nd$  states ( $n = 35, 36, 37$  and  $n = 48, 49, 50$ ) is shown. (b) Zoomed-in portion of the spectrum showing  $36d$  and  $38s$  corresponding to the green highlighted part of (a). The broad and narrow peak features of the  $nd$  and  $ns$  states are visible. Error bars indicate the standard deviation of three repeated measurements. The red line (blue line) represents the result of the fit of a Gaussian line profile to the measured  $36d$  ( $38s$ ) data points.

Each of the data points is recorded three times and the spectrum along with the standard deviation is shown in Fig. 2(a). It shows the remaining number of atoms as a function of the frequency of the coupling laser. We can see a peak due to reduced atom loss when the coupling laser is tuned in resonance with a particular Rydberg level. The Rydberg spectrum portion of Fig. 2(b) contains a narrow and a broad peak corresponding to the  $ns$  and  $nd$  resonances, respectively. The reason for

the different linewidth of the resonances is the different dc polarizabilities of the  $ns$  and  $nd$  states; the polarizability of the  $nd$  states is approximately five times larger than for the  $ns$  states [40]. The spectrum of Fig. 2 shows some parts of the peaks below the  $n = 63$ , and the remaining detected peaks of the spectrum are listed in Table I. The theoretical values of the peaks in Table I were calculated from Ref. [45]. The values in parentheses of the experimental data in Table I are from the fit

TABLE I. Transition portion of  $4p_{3/2} \rightarrow ns$  and  $4p_{3/2} \rightarrow nd$  of  $^{40}\text{K}$  ultracold Fermi gases in theory and experiment. The detectable highest Rydberg state in our experiment is  $n = 62$  limited by the competition between the Rydberg blockade effective range and the atomic cloud size. Here  $n$  is principal quantum number and the theoretical value of the transition was calculated by Ref. [45]. The values in parentheses of the experimental data were from the fit in Figs. 2 and 3, and represent the detection's resolution.

$n$	Theory	$4p_{3/2} \rightarrow ns$ (THz) Case1/case2 (Expt.)	$\delta_s$	Theory	$4p_{3/2} \rightarrow nd$ (THz) Case1/case2 (Expt.)	$\delta_d$
$\vdots$	$\vdots$	$\vdots$	$\vdots$	$\vdots$	$\vdots$	$\vdots$
34	655.302943			655.659524		
35	655.497931			655.823724	655.82316(1.7) / 655.82248(7.4)	0.276/0.280
36	655.675880			655.974331	655.97318(1.6) / 655.97315(4.3)	0.280/0.280
37	655.838719	655.83822(4.7) / 655.83786(3.6)	2.179/2.182	656.112803	656.11210(5.4) / 656.11165(8.2)	0.277/0.280
38	655.988110	655.98759(1.1) / 655.98717(2.6)	2.180/2.182	656.240411		
39	656.125495	656.12488(9.8) / 656.12470(1.1)	2.180/2.182	656.358262		
$\vdots$	$\vdots$	$\vdots$	$\vdots$	$\vdots$	$\vdots$	$\vdots$
48	656.985171			657.107695	657.10660(1.7)/657.10626(4.4)	0.284/0.290
49	657.051393			657.166377	657.16522(2.8)/657.16448(6.2)	0.286/0.299
50	657.113505	657.11285(5.7) / 657.11219(4.6)	2.181/2.192	657.221555	657.22029(3.5)/657.22020(1.0)	0.288/0.290
51	657.171838	657.17111(1.2) / 657.17088(1.0)	2.182/2.186	657.273502		
52	657.226695	657.22595(2.2) / 657.22548(4.1)	2.182/2.191	657.322465		
53	657.278345			657.368669		
54	657.327033			657.412317		
$\vdots$	$\vdots$	$\vdots$	$\vdots$	$\vdots$	$\vdots$	$\vdots$
60	657.568104			657.629834	-/657.62722(10)	-/0.341
61	657.601280			657.659961		
62	657.632805	-/657.63169(12)	-/2.196	657.688636		
$\vdots$	$\vdots$	$\vdots$	$\vdots$	$\vdots$	$\vdots$	$\vdots$

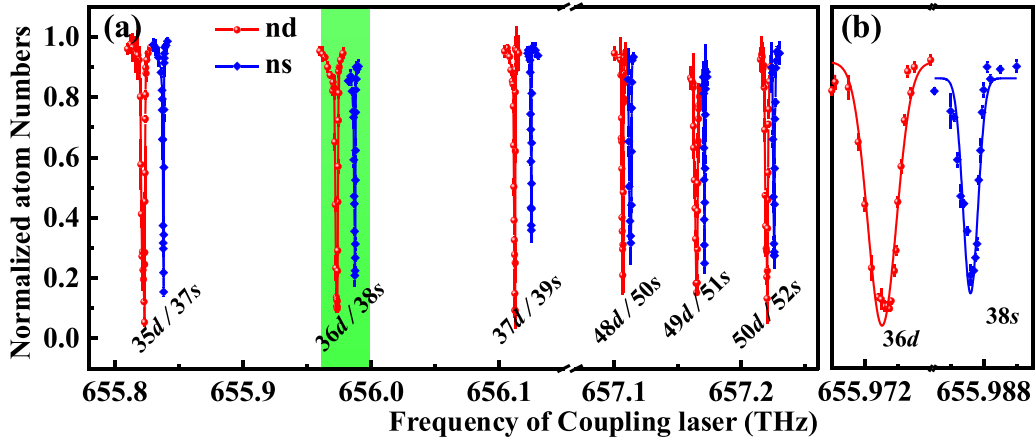


FIG. 3. Rydberg spectrum of ultracold  $^{40}\text{K}$  atoms by the avalanche ionization scheme. (a) The Rydberg loss spectrum recorded with strongly focused probe field. The results agree with the spectrum of the weak probe EIT spectrum very well. (b) Zoomed-in portion of the spectrum showing  $36d$  and  $38s$  as dips corresponding to the green highlighted part of Fig. 3(a). Error bars indicate the standard deviation of three repeated measurements. The red line (blue line) represents the result of the fit of a Gaussian line profile to the measured  $36d$  ( $38s$ ) data points.

in Fig. 2 and Fig. 3, and represent the uncertainty, which arises from variations in parameters and fluctuations in the measured signal during the scans [40].

Next, we measure the Rydberg spectrum using a high power probe field to enhance the atomic losses by spontaneous avalanche ionization of the strong Rydberg-Rydberg interactions. Under strong laser excitation, a Rydberg ensemble is created in the strong blockade regime, which undergoes an ionization avalanche, including the rapid increase in the number of ions and a sudden depletion of the Rydberg and ground-state densities. The probe field in this scheme is provided by another beam along the  $y$  axis, which is strong focused to a  $1/e^2$  waist of  $w_0 = 4 \mu\text{m}$  by a high-NA aspheric lens (ASL10142-B) with focal length 79 mm, while the coupling beam is the same as in the previous case, as shown in Fig. 1(c). The *in situ* atomic density profile presents a hole at the center [inset of Fig. 1(c1)] corresponding to the atomic losses induced by the strongly focused probe light. The intensities of the probe and coupling fields are around  $1.99 \times 10^{-2} \text{ W/mm}^2$  and  $19 \text{ W/mm}^2$ , respectively. The time sequence is also the same as in the previous case but the atoms are imaged by *in situ* imaging with the same high-NA aspheric lens (without any TOF) using a laser beam along the  $y$  axis [51].

As shown in Fig. 3(a), the spectrum recorded using this method shows enhanced atom loss (the avalanche ionization scheme) as a function of the coupling laser frequency. The results agree with the spectrum of the weak probe EIT spectrum (Fig. 2) very well. We can see from the Rydberg spectrum portion of Fig. 3(b) a narrow and a broad dip corresponding to the  $ns$  and  $nd$  resonances, respectively [40]. This behavior is shared by all the  $ns$  and  $nd$  resonances in the spectrum.

Furthermore, we have also observed an additional broad resonance of a  $62p^-$  state, which is the dipole-forbidden transition as shown in Fig. 4. This case is only for the higher Rydberg states. We surmise that these forbidden transitions are visible because the weak residual electric fields in the experiment induce the mixing of the states with different parity [40]. This mixing is more favorable for the higher Rydberg states.

In conclusion, we have measured the Rydberg excitation spectrum through a two-photon process of the ultracold  $^{40}\text{K}$  atoms in the ladder-type system using two different methods. The natural abundance of fermionic  $^{40}\text{K}$  is very low and, therefore, the measurement of Rydberg excitation spectra for fermionic  $^{40}\text{K}$  atoms in a natural abundance vapor cell is not easy to perform. Our work provides an experimental study of the Rydberg excitation spectra of the degenerate fermionic  $^{40}\text{K}$  atoms. The EIT detection scheme reduces atomic losses due to reduced absorption for the weak probe light, while the avalanche ionization scheme enhances the atomic losses by spontaneous avalanche ionization for the strong probe light. We have observed the narrow  $ns$  and broad  $nd$  features in the spectrum of the excited Rydberg states. We also measured the additional broad resonance of the  $np^-$  state only for the higher Rydberg states, which is the dipole-forbidden transition. This work takes a first step in studying Rydberg-dressed

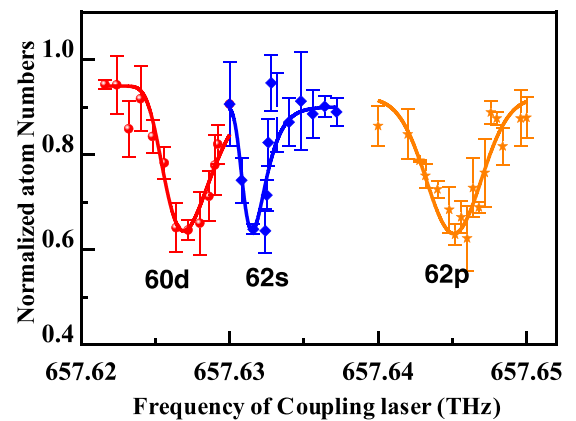


FIG. 4. Rydberg spectrum of  $60d$ ,  $62s$ , and  $62p$  states by the enhanced atomic losses detection method. We find that the detectable highest Rydberg state in our experiment is  $n \leq 62$ . The dipole-forbidden transition to the  $62p$  state is also visible in the spectrum. Error bars indicate the standard deviation of three repeated measurements.

$^{40}\text{K}$  ultracold Fermi gases, and it can help in the study of interesting phenomena related to the dressed ultracold Fermi gases like the many-body phase diagram and the observation of continuous supersolids involving Rydberg states. Moreover, the spontaneous avalanche ionization technique can generate ultracold, strongly coupled plasmas that can be useful for the exploration of the nonequilibrium dynamics.

This research is supported by National Key Research and Development Program of China (Grants No. 2016YFA0301602 and No. 2018YFA0307601), National Natural Science Foundation of China (Grants No. 12034011, No. 92065108, No. 11804203, No. 11974224, No. 12022406, and No. 12004229), and the Fund for Shanxi 1331 Project Key Subjects Construction.

- 
- [1] T. F. Gallagher, *Rydberg Atoms* (Cambridge University Press, Cambridge, UK, 1994).
- [2] D. Comparat and P. Pillet, Dipole blockade in a cold Rydberg atomic sample, *J. Opt. Soc. Am. B* **27**, A208 (2010).
- [3] E. Urban, T. A. Johnson, T. Henage, L. Isenhower, D. D. Yavuz, T. G. Walker, and M. Saffman, Observation of Rydberg blockade between two atoms, *Nat. Phys.* **5**, 110 (2009).
- [4] C. H. Greene, A. S. Dickinson, and H. R. Sadeghpour, Creation of Polar and Nonpolar Ultra-Long-Range Rydberg Molecules, *Phys. Rev. Lett.* **85**, 2458 (2000).
- [5] D. Booth, S. T. Rittenhouse, J. Yang, H. R. Sadeghpour, and J. P. Shaffer, Production of trilobite Rydberg molecule dimers with kilo-Debye permanent electric dipole moments, *Science* **348**, 99 (2015).
- [6] M. T. Eiles, Trilobites, butterflies, and other exotic specimens of long-range Rydberg molecules, *J. Phys. B: At., Mol., Opt. Phys.* **52**, 113001 (2019).
- [7] E. L. Hamilton, C. H. Greene, and H. R. Sadeghpour, Shape-resonance-induced long-range molecular Rydberg states, *J. Phys. B: At., Mol., Opt. Phys.* **35**, L199 (2002).
- [8] T. Niederprüm, O. Thomas, T. Eichert, C. Lippe, J. Pérez-Ríos, C. H. Greene, and H. Ott, Observation of pendular butterfly Rydberg molecules, *Nat. Commun.* **7**, 12820 (2016).
- [9] C. Boisseau, I. Simbotin, and R. Côté, Macrodimers: Ultralong Range Rydberg Molecules, *Phys. Rev. Lett.* **88**, 133004 (2002).
- [10] S. M. Farooqi, D. Tong, S. Krishnan, J. Stanojevic, Y. P. Zhang, J. R. Ensher, A. S. Estrin, C. Boisseau, R. Côté, E. E. Eyler, and P. L. Gould, Long-Range Molecular Resonances in a Cold Rydberg Gas, *Phys. Rev. Lett.* **91**, 183002 (2003).
- [11] S. Hollerith, J. Zeiher, J. Rui, A. Rubio-Abadal, V. Walther, T. Pohl, D. M. Stamper-Kurn, I. Bloch, and C. Gross, Quantum gas microscopy of Rydberg macrodimers, *Science* **364**, 664 (2019).
- [12] H. Saßmannshausen and J. Deiglmayr, Observation of Rydberg-Atom Macrodimers: Micrometer-Sized Diatomic Molecules, *Phys. Rev. Lett.* **117**, 083401 (2016).
- [13] X. Han, S. Bai, Y. Jiao, L. Hao, Y. Xue, J. Zhao, S. Jia, and G. Raithel, Cs  $62D_7$  Rydberg-atom macrodimers formed by long-range multipole interaction, *Phys. Rev. A* **97**, 031403(R) (2018).
- [14] A. Browaeys and T. Lahaye, Many-body physics with individually controlled Rydberg atoms, *Nat. Phys.* **16**, 132 (2020).
- [15] I. Buluta and F. Nori, Quantum simulators, *Science* **326**, 108 (2009).
- [16] H. Weimer, M. Müller, I. Lesanovsky, P. Zoller, and H. P. Büchler, A Rydberg quantum simulator, *Nat. Phys.* **6**, 382 (2010).
- [17] L. Henriot, L. Beguin, A. Signoles, T. Lahaye, A. Browaeys, G.-O. Reymond, and C. Jurczak, Quantum computing with neutral atoms, *Quantum* **4**, 327 (2020).
- [18] M. Morgado and S. Whitlock, Quantum simulation and computing with Rydberg-interacting qubits, *AVS Quantum Sci.* **3**, 023501 (2021).
- [19] X. Wu, X. Liang, Y. Tian, F. Yang, C. Chen, Y.-C. Liu, M. K. Tey, and L. You, A concise review of Rydberg atom based quantum computation and quantum simulation, *Chin. Phys. B* **30**, 020305 (2021).
- [20] T. C. Liebisch, M. Schlagmüller, F. Engel, H. Nguyen, J. Balewski, G. Lochead, F. Böttcher, K. M. Westphal, K. S. Kleinbach, T. Schmid, A. Gaj, R. Löw, S. Hofferberth, T. Pfau, J. Pérez-Ríos, and C. H. Greene, Controlling Rydberg atom excitations in dense background gases, *J. Phys. B: At., Mol., Opt. Phys.* **49**, 182001 (2016).
- [21] J. Sous, H. R. Sadeghpour, T. C. Killian, E. Demler, and R. Schmidt, Rydberg impurity in a Fermi gas: Quantum statistics and rotational blockade, *Phys. Rev. Research* **2**, 023021 (2020).
- [22] J. D. Whalen, S. K. Kanungo, R. Ding, M. Wagner, R. Schmidt, H. R. Sadeghpour, S. Yoshida, J. Burgdörfer, F. B. Dunning, and T. C. Killian, Probing nonlocal spatial correlations in quantum gases with ultra-long-range Rydberg molecules, *Phys. Rev. A* **100**, 011402(R) (2019).
- [23] J. B. Balewski, A. T. Krupp, A. Gaj, S. Hofferberth, R. Löw, and T. Pfau, Rydberg dressing: Understanding of collective many-body effects and implications for experiments, *New J. Phys.* **16**, 063012 (2014).
- [24] C. Gaul, B. J. DeSalvo, J. A. Aman, F. B. Dunning, T. C. Killian, and T. Pohl, Resonant Rydberg Dressing of Alkaline-Earth Atoms Via Electromagnetically Induced Transparency, *Phys. Rev. Lett.* **116**, 243001 (2016).
- [25] A. Gaëtan, Y. Miroshnychenko, T. Wilk, A. Chotia, M. Viteau, D. Comparat, P. Pillet, A. Browaeys, and P. Grangier, Observation of collective excitation of two individual atoms in the Rydberg blockade regime, *Nat. Phys.* **5**, 115 (2009).
- [26] R. Heidemann, U. Raitzsch, V. Bendkowsky, B. Butscher, R. Low, and T. Pfau, Rydberg Excitation of Bose-Einstein Condensates, *Phys. Rev. Lett.* **100**, 033601 (2008).
- [27] M. Viteau, M. Bason, J. Radogostowicz, N. Malossi, O. Morsch, D. Ciampini, and E. Arimondo, Rydberg excitation of a Bose-Einstein condensate, *Laser Phys.* **23**, 015502 (2013).
- [28] P. Schauß, J. Zeiher, T. Fukuhara, S. Hild, M. Cheneau, T. Macri, T. Pohl, I. Bloch, and C. Gross, Crystallization in Ising quantum magnets, *Science* **347**, 1455 (2015).
- [29] J. Zeiher, J.-y. Choi, A. Rubio-Abadal, T. Pohl, R. van Bijnen, I. Bloch, and C. Gross, Coherent Many-Body Spin Dynamics in a Long-Range Interacting Ising Chain, *Phys. Rev. X* **7**, 041063 (2017).
- [30] V. Borish, O. Marković, J. A. Hines, S. V. Rajagopal, and M. Schleier-Smith, Transverse-Field Ising Dynamics in a Rydberg-Dressed Atomic Gas, *Phys. Rev. Lett.* **124**, 063601 (2020).



- [31] J. Zeiher, R. van Bijnen, P. Schauß, S. Hild, J.-y. Choi, T. Pohl, I. Bloch, and C. Gross, Many-body interferometry of a Rydberg-dressed spin lattice, *Nat. Phys.* **12**, 1095 (2016).
- [32] Y.-Y. Jau, A. M. Hankin, T. Keating, I. H. Deutsch, and G. W. Biedermann, Entangling atomic spins with a Rydberg-dressed spin-flip blockade, *Nat. Phys.* **12**, 71 (2016).
- [33] B. Xiong, H. H. Jen, and D.-W. Wang, Topological superfluid by blockade effects in a Rydberg-dressed Fermi gas, *Phys. Rev. A* **90**, 013631 (2014).
- [34] W.-H. Li, T.-C. Hsieh, C.-Y. Mou, and D.-W. Wang, Emergence of a Metallic Quantum Solid Phase in a Rydberg-Dressed Fermi Gas, *Phys. Rev. Lett.* **117**, 035301 (2016).
- [35] X. Li and S. D. Sarma, Exotic topological density waves in cold atomic Rydberg-dressed fermions, *Nat. Commun.* **6**, 7137 (2015).
- [36] A. Keleş, E. Zhao, and X. Li,  $f$ -wave superfluidity from repulsive interaction in Rydberg-dressed fermi gas, *Phys. Rev. A* **101**, 023624 (2020).
- [37] R. Khasseh, S. H. Abedinpour, and B. Tanatar, Phase diagram and dynamics of Rydberg-dressed fermions in two dimensions, *Phys. Rev. A* **96**, 053611 (2017).
- [38] M. Mattioli, M. Dalmonte, W. Lechner, and G. Pupillo, Cluster Luttinger Liquids of Rydberg-Dressed Atoms in Optical Lattices, *Phys. Rev. Lett.* **111**, 165302 (2013).
- [39] W. Xu and B. DeMarco, Velocity-selective electromagnetically-induced-transparency measurements of potassium Rydberg states, *Phys. Rev. A* **93**, 011801(R) (2016).
- [40] A. Arias, S. Helmrich, C. Schweiger, L. Ardizzone, G. Lochead, and S. Whitlock, Versatile, high-power 460 nm laser system for Rydberg excitation of ultracold potassium, *Opt. Express* **25**, 14829 (2017).
- [41] M. Peper, F. Helmrich, J. Butscher, J. A. Agner, H. Schmutz, F. Merkt, and J. Deiglmayr, Precision measurement of the ionization energy and quantum defects of  $^{39}\text{K}$ , *Phys. Rev. A* **100**, 012501 (2019).
- [42] M. Fleischhauer, A. Imamoglu, and J. P. Marangos, Electromagnetically induced transparency: Optics in coherent media, *Rev. Mod. Phys.* **77**, 633 (2005).
- [43] T. M. Weber, T. Niederprüm, T. Manthey, P. Langer, V. Guarrera, G. Barontini, and H. Ott, Continuous coupling of ultracold atoms to an ionic plasma via Rydberg excitation, *Phys. Rev. A* **86**, 020702(R) (2012).
- [44] M. Robert-de-Saint-Vincent, C. S. Hofmann, H. Schempp, G. Günter, S. Whitlock, and M. Weidemüller, Spontaneous Avalanche Ionization of a Strongly Blockaded Rydberg Gas, *Phys. Rev. Lett.* **110**, 045004 (2013).
- [45] N. Šibalić, J. Pritchard, C. Adams, and K. Weatherill, Arc: An open-source library for calculating properties of alkali Rydberg atoms, *Comput. Phys. Commun.* **220**, 319 (2017).
- [46] A. K. Mohapatra, T. R. Jackson, and C. S. Adams, Coherent Optical Detection of Highly Excited Rydberg States Using Electromagnetically Induced Transparency, *Phys. Rev. Lett.* **98**, 113003 (2007).
- [47] K.-J. Boller, A. Imamoglu, and S. E. Harris, Observation of Electromagnetically Induced Transparency, *Phys. Rev. Lett.* **66**, 2593 (1991).
- [48] C. Y. Ye and A. S. Zibrov, Width of the electromagnetically induced transparency resonance in atomic vapor, *Phys. Rev. A* **65**, 023806 (2002).
- [49] A. Monden, EIT spectroscopy on rubidium Rydberg states, Master's thesis, Eindhoven University of Technology, 2015.
- [50] B. D. Yang, J. Gao, J. Wang, T. C. Zhang, and J. M. Wang, Multiple electromagnetically-induced transparency of hyperfine levels in cesium  $6s1/2$  -  $6p3/2$  -  $8s1/2$  ladder-type system, *Acta Phys. Sin.* **60**, 114207 (2011).
- [51] W. S. Bakr, J. I. Gillen, A. Peng, S. Fölling, and M. Greiner, A quantum gas microscope for detecting single atoms in a Hubbard-regime optical lattice, *Nature (London)* **462**, 74 (2009).